Microbubble embedded with upconversion nanoparticles as a bimodal contrast agent for fluorescence and ultrasound imaging

2015 Nanotechnology 26 345601

(http://iopscience.iop.org/0957-4484/26/34/345601)

IOP Publishing Nanotechnology
Nanotechnology **26** (2015) 345601 (8pp) doi:10.1088/0957-4484/26/34/345601

Microbubble embedded with upconversion nanoparticles as a bimodal contrast agent for fluorescence and ultrasound imaging

Birui Jin[1,2], Min Lin[2,3,4], Minli You[2,3], Yujin Zong[3], Mingxi Wan[3], Feng Xu[2,3], Zhenfeng Duan[4] and Tianjian Lu[2]

[1] State Key Laboratory for Mechanical Behavior of Materials, Xi'an Jiaotong University, Xi'an 710049, People's Republic of China
[2] Bioinspired Engineering and Biomechanics Center (BEBC), Xi'an Jiaotong University, Xi'an 710049, People's Republic of China
[3] MOE Key Laboratory of Biomedical Information Engineering, Xi'an Jiaotong University, Xi'an 710049, People's Republic of China
[4] Center for Sarcoma and Connective Tissue Oncology, Massachusetts General Hospital, Harvard Medical School, MA 02114, USA

E-mail: minlin@mail.xjtu.edu.cn and tjlu@mail.xjtu.edu.cn

Received 29 March 2015, revised 19 June 2015
Accepted for publication 3 July 2015
Published 5 August 2015

Abstract

Bimodal imaging offers additional imaging signal thus finds wide spread application in clinical diagnostic imaging. Fluorescence/ultrasound bimodal imaging contrast agent using fluorescent dyes or quantum dots for fluorescence signal has emerged as a promising method, which however requires visible light or UV irradiation resulting in photobleaching, photoblinking, auto-fluorescence and limited tissue penetration depth. To surmount these problems, we developed a novel bimodal contrast agent using layer-by-layer assembly of upconversion nanoparticles onto the surface of microbubbles. The resulting microbubbles with average size of 2 μm provide enhanced ultrasound echo for ultrasound imaging and upconversion emission upon near infrared irradiation for fluorescence imaging. The developed bimodal contrast agent holds great potential to be applied in ultrasound target technique for targeted diseases diagnostics and therapy.

Keywords: ultrasound, microbubbles, bimodal contrast agent, upconversion, layer-by-layer self-assembly

(Some figures may appear in colour only in the online journal)

1. Introduction

Ultrasound imaging has been widely applied in clinics due to several advantages associated with low-cost [1], convenience [2], safety to the body [3] and real-time imaging in deep tissue [4]. However, ultrasound imaging suffers from low contrast as compared to other imaging techniques such as x-ray tomography, computed tomography (CT) and magnetic resonance imaging (MRI) [5]. To address this issue, various ultrasound contrast agents are employed to enhance imaging contrast, among which microbubbles (MBs) have received intensive study since MBs with diameter ranging between $1 \sim 10\,\mu$m (similar to erythrocytes) can be injected in the vein and pass through the circulatory system [6–9]. MBs could significantly enhance backscatter acoustic signal due to the resonance induced by the different acoustic impedance between the MBs and the tissues [10, 11]. However, ultrasound imaging as single-mode imaging can only provide a single imaging signal. To address this, surface functionalization of MBs has been performed to achieve bimodal or multi-modal imaging for improved accuracy of clinical assessment of diseases, for example, after conjugation with an antibody, the MBs are capable of targeted molecular imaging [12, 13]. Additionally, a bimodal contrast agent that combines

MRI and ultrasound imaging signals has been demonstrated in superparamagnetic nanoparticles and MBs composite system [14, 15]. Fluorescence-particle-modified MBs have also been reported as another promising bimodal contrast agent [16, 17].

Various fluorescence materials including fluorescence dyes and quantum dots (QDs) have been combined with MBs to achieve fluorescence/ultrasound bimodal imaging [16, 18]. Although fluorescence dyes have the advantages of low cost, good biocompatibility, and easy preparation [19], their applications have been limited by low photostability, auto-fluorescence, and easy quenching [20]. In comparison, QDs have been widely applied for fluorescence/ultrasound bimodal imaging due to their excellent optical performance (e.g., no photobleaching, high photostability, tunable emission band) [16, 17, 21]. However, cadmium from QDs involves the issue of significant cytotoxicity [22] and the required UV excitation involves the potential issue of tissue damage, auto-fluorescence, and limited tissue penetration [23]. Therefore, there is still an unmet need for development of fluorescence/ultrasound bimodal imaging probes that avoid the associated limitations.

Lanthanide (Ln)-doped upconversion nanoparticles (UCNPs) exhibit the unique fluorescence property of converting excitation to visible emission [23]. Compared with fluorescence dyes and QDs, UCNPs offer several advantages such as non-photobleaching, non-photoblinking [24], and low cytotoxicity to a broad range of cell lines [23]. In addition, NIR excitation produces negligible photo-damage to biological specimens (e.g., RNA, DNA) [25], high signal to noise ratio [20], and deep tissue penetration capacity [26]. The combination of UCNPs with MBs will produce advanced fluorescence/ultrasound bimodal contrast agent for bioimaging. However, this has not been explored yet.

In this study, we developed a novel approach to prepare a fluorescence/ultrasound contrast agent for bimodal imaging by embedding UCNPs onto the surface of MBs using a layer-by-layer (LbL) assembly technique. Besides providing an additional upconversion fluorescence signal, embedding of UCNPs onto the MBs surface also enhanced the ultrasound echo of the MB itself. With this study, we greatly increase the availability of fluorescence/ultrasound imaging in biological applications.

2. Results and discussion

2.1. Materials

$YCl_3 \cdot 6H_2O$, $YbCl_3 \cdot 6H_2O$, $ErCl_3 \cdot 6H_2O$, $GdCl_3 \cdot 6H_2O$, NH_4F, Sorbitan monostearate (Span 60, M.W. 431), and polyoxyethy-lene sorbitan monooleate (Tween 80, M.W. 1307) were purchased from Sigma Aldrich. 1-Octacene (90%) sodium and oleic acid (90%) were obtained from Alfa Aesar. Methanol, chloroform, ethanol, and NaOH were obtained from Tianjinzhiyuan Chemical Reagen Co., Ltd Poly(allylamine hydrochloride) (PAH, M.W. ~56000) and poly(acrylic acid) (PAA, Mw = 800–1000) were obtained from Tianjinyongsheng Chemical Reagen Co., Ltd SF_6 gas was obtained from Liming Research Institute of Chemical Industry. Phosphate buffer saline (PBS, pH = 7.4) was prepared by 8.010 g NaCl, 0.194 g KCl, 2.290 g $Na_2HPO_4 \cdot 12H_2O$, and 0.191 g KH_2PO_4 in 1 L water. All reagents were of analytical grade and were used without any purification.

2.2. Synthesis of $NaYF_4$:Yb/Er UCNPs

The synthesis of UCNPs was carried out by a thermal decomposition procedure according to reported protocol [27, 28]. In a typical synthesis of 30 nm sized β-$NaYF_4$:Er/Yb, $YCl_3 \cdot 6H_2O$ (242.69 mg, 0.8 mmol), $YbCl_3 \cdot 6H_2O$ (69.75 mg, 0.18 mmol), and $ErCl_3 \cdot 6H_2O$ (7.64 mg, 0.02 mmol) were dissolved in 2 mL deionized water and were then added to a 100 mL flask containing 7.5 mL oleic acid and 15 mL 1-octadecene. The solution was stirred at room temperature for 0.5 h. Afterwards, the mixture was slowly heated to 120 °C and then kept for 1 h at 156 °C to get rid of water under argon atmosphere. The system was then cooled down to room temperature. 10 mL methanol solution of NH_4F (148.15 mg, 4 mmol) and NaOH (100 mg, 2.5 mmol) were added and the solution was stirred at room temperature for 2 h. After methanol evaporation, the solution was heated to 280 °C and maintained for 1.5 h, then cooled down to room temperature. The resulting product was washed with ethanol and cyclohexane three times and was finally re-dispersed in 10 mL cyclohexane.

2.3. Surface modification by PAA

A ligand exchange process was performed using PAA as a multidentate ligand that displaces the original hydrophobic ligands on the UCNPs surface by mixing 14.5 μL PAA, 1 mL ethanol, and 1 mL of UCNPs dispersed in chloroform (~15 mg mL^{-1}) with overnight stirring. The solution was then centrifuged at 10 000 rpm for 10 min. After being washed three times with ethanol and deionized water, the particles were re-dispersed in 5 mL deionized water.

2.4. Preparation of ST68 MBs

ST68 MBs were prepared according to reported protocol [29]. Briefly, 1.48 g Span 60 and 1.5 g NaCl were mixed in 50 mL PBS. 1 mL Tween 80 was added to the solution and was stirred at 40 °C until the solution was well mixed. Then the mixture was sonicated continuously by a 12 mm diameter titanium alloy horn (Sonicator VCX-750) with 75% maximum output amplitude setting under the atmosphere of SF_6 gas for 3 min The resulting suspension was allowed to stand for about 3 h to separate into three layers. The middle layer was collected and washed three times by PBS. The obtained MBs were 1:1 (v:v) suspended in PBS, protected by SF_6 gas, sealed, and stored at 4 °C.

2.5. Modification of ST68 MBs with UCNPs

PAH solution was prepared with a concentration of 1.0 mg mL^{-1} containing 0.5 mol L^{-1} NaCl. The 5 mL PAH

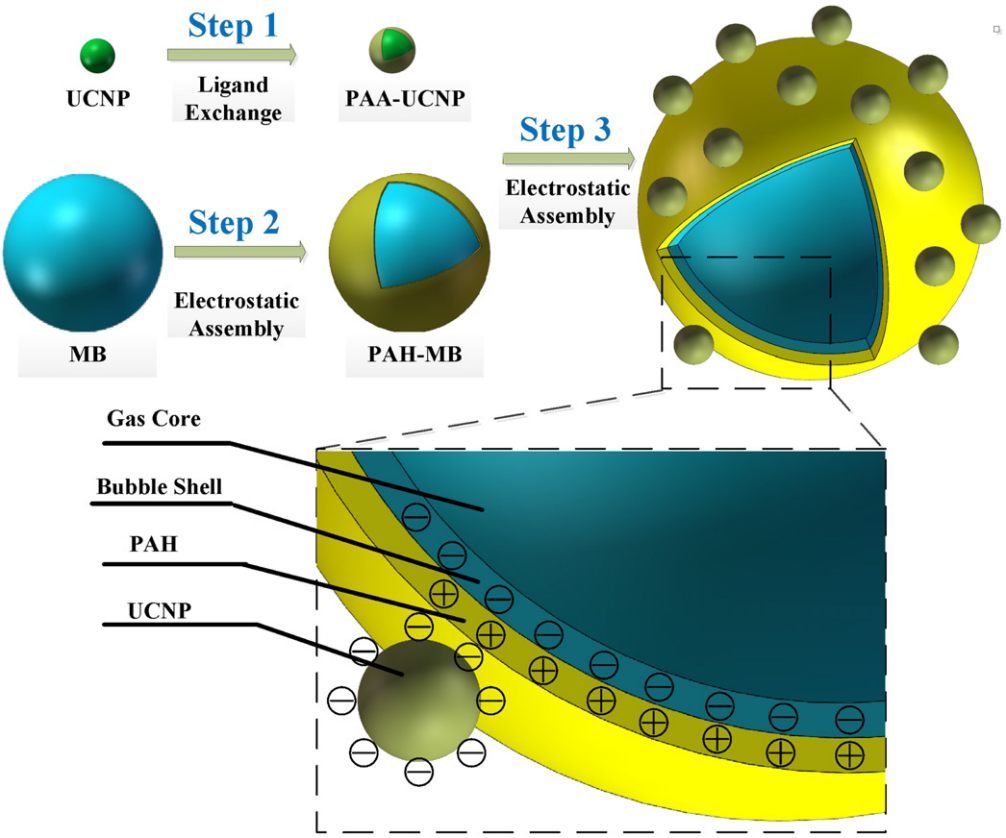

Figure 1. Schematic of loading UCNPs to MBs by LbL assembly method. Step 1: the ligand exchange method is used for PAA coating UCNPs, the obtained PAA-UCNPs are negatively charged. Step 2: the positively charged PAH are electrostatically assembled onto MBs with negative charge surface. Step 3: UCNPs are electrostatically assembled onto the surface modification MBs.

solution was added to the separating funnel, which contained 3 mL ST68 suspension. The suspension was then slightly shaken for 15 min to make sure the PAH sufficiently adsorpted to surface of MBs. MBs were allowed to float to the top layer of the suspension, leaving the excessive polyelectrolytes in the bottom layer that was then discarded. The MBs were then re-suspended and washed by PBS three times. Thereafter, 5 mL 20-time-diluted PAA-UCNPs solution was added and the excessive PAA-UCNPs were discarded using the similar mix-stand-wash steps. The produced UCNP@ST68 MBs were 1:1 (v:v) suspended in PBS, protected by SF_6 gas, sealed, and stored at 4 °C.

2.6. Material characterizations

The morphology of ST68 MBs was imaged by optical microscope (Olympus IX2-UCB). The size distribution was analyzed by Image J software. The concentration of the MBs was calculated by a hemocytometer. A fluorescence spectrophotometer (Quanta Master TM40) was used to access the fluorescence spectrum of UCNPs. The excitation wavelength of 980 nm was provided by a laser diode with power density of 250 mW 980 nm (RGB Lasersystems). A FT-IR (Thermo IS50) was used to prove successful coating of PAA on UCNPs. The conjugation of UCNPs and MBs was confirmed by a fluorescence microscope by both fluorescence mode and bright-field mode (Olympus IX2-UCB).

2.7. In vitro ultrasound imaging

The *in vitro* ultrasound imaging capability of the MBs before and after UCNPs coating was evaluated using a latex tube simulating the blood vessel phantom immersed in a water tank. An ultrasound probe was positioned closely to the tube. Ultrasound imaging was taken by ultrasound system (Mindray DC-6). The ultrasound frequency was fixed at 5 MHz and the acoustic pressure was estimated to be around 300 kPA. The ultrasound imaging was obtained by adjusting gain value to be 55%.

3. Results and discussion

To combine UCNPs onto the surface of MBs, we developed a LbL assembly approach (figure 1). The bimodal MBs were prepared by the assembly of ST68 MBs in an aqueous solution with stepwise LbL assembly of PAH and PAA-UCNPs onto the surface of the MBs. First, SF_6-filled MBs were generated by mixing Span 60 and Tween 80 in PBS, followed by sonicating according to the reported procedure [29]. The suspension was allowed to separate into three layers, and the middle layer was collected since this layer is mostly populated by MBs with appropriate size ranging between 1 and 10 μm (larger bubbles were mostly in the top layer and smaller bubbles and excessive surfactant were in the bottom

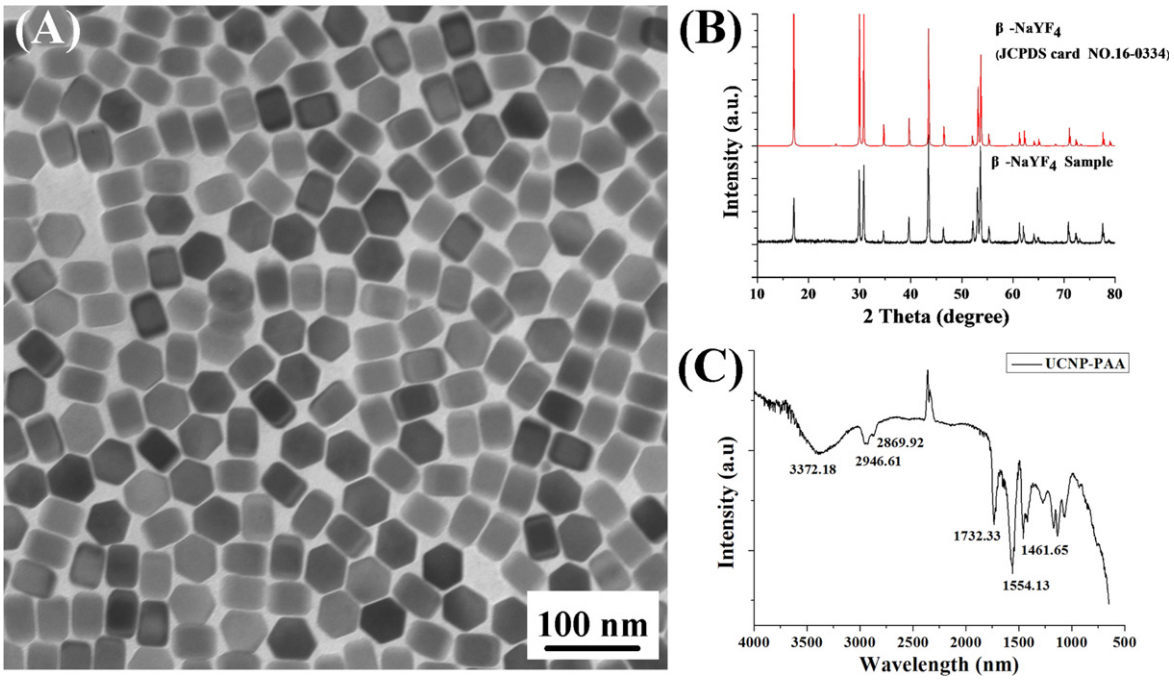

Figure 2. Characterization of UCNPs. (a) TEM image of UCNPs, (b) XRD pattern of UCNPs, and (c) FR-IT spectrum of PAA-UCNPs.

layer). The prepared MBs were negatively charged [17]. Then, the LbL assembly was processed by alternatively depositing positive-charged PAH and negative-charged PAA-UCNPs. The products were washed by PBS three times after assembly of each layer.

The $NaYF_4$:Yb/Er nanoparticles used in this study were synthesized using a thermal decomposition route in the presence oleic acid. The mean diameter of the synthesized nanoparticles is ~35 nm (figure 2(a)). The XRD pattern of the product (figure 2(b)) shows that all the diffraction peaks can be ascribed to the hexagonal structure of $NaYF_4$ (JCPDS no. 16-0334). The PAA functionalized UCNPs were further verified by FT-IR spectroscopy (figure 2(c)). We observed a broad band at approximately 3372 cm^{-1}, which corresponds to the O-H stretching vibration. The transmission bands at 2946 and 2869 cm^{-1} can be respectively assigned to the asymmetric and symmetric stretching vibrations of the methylene (-CH2-) in the long alkyl chain. We also observed two strong bands centered at 1554 and 1461 cm^{-1}, which could be associated with the asymmetric and symmetric stretching vibrations of carboxylate anions on the surface of the UCNPs before the ligand exchange.

To prepare MBs, sonication is applied for surfactant film formation. However, the resulting diameter of the bubbles ranges between hundreds of microns and nanometers [30]. One of the essential features of MBs for clinical applications is the size. MBs with size exceeding 10 μm are not able to access the pulmonary capillaries and do great harm to the body [31, 32]. Smaller-sized MBs (nanometer size) are able to penetrate through blood capillary for imaging, but suffer from relatively weak ability to enhance contrast [33, 34]. Experimental evidence shows that the most appropriate MB size is between 1–10 μm [35, 36]. To obtain the appropriate MB size, we collected the middle layer after standing. The collected sample was subjected to optical microscope observation (figure 3(a)). The size distribution is shown in figure 3(b). The estimated average size of the MBs is 2.36 ± 1.15 μm. Since the size of MBs is similar to erythrocytes, the concentration of the MBs can therefore be analyzed using a hemocytometer. The obtained concentration is 7×10^8 bubbles/mL.

To prove the successful assembly of UCNPs onto the surface of MBs, we checked the morphology of UCNP@ST68 in both bright-field mode (figure 3(c)) and fluorescence mode (figure 3(d)) under an optical microscope. Under bright-field mode, all the MBs maintain their spherical structure (figure 3(c)). From the same microscopic field in fluorescence mode under an external 980 nm laser excitation, the green fluorescence could be seen on the surface of every individual MB (figure 3(d)). This indicates that UCNPs could successfully deposit on the surface of MBs via LbL assembly technology. Some of the UCNP@ST68 MBs do not show an intact spherical structure in the fluorescent mode. This may be attributed to the incomplete adsorption or non-uniform distribution of UCNPs on the surface of the MBs. UCNP@ST68 MBs have the same morphology and size as ST68 MBs (figures 3(a) and (c)). This demonstrates that the MBs are stable during the process of combining UCNPs onto the surface of MBs.

The inset of figure 4 shows the photograph of the as-prepared UCNP@ST68 MBs. The MBs in the bottle are separated into two layers: the bottom layer is PBS, which is clear, and the top layer is the gathered MBs. Under 980 nm excitation, only the top layer presents green fluorescence and the bottom layer shows no fluorescence, which indicates that UCNPs are well modified onto the surface of the MBs

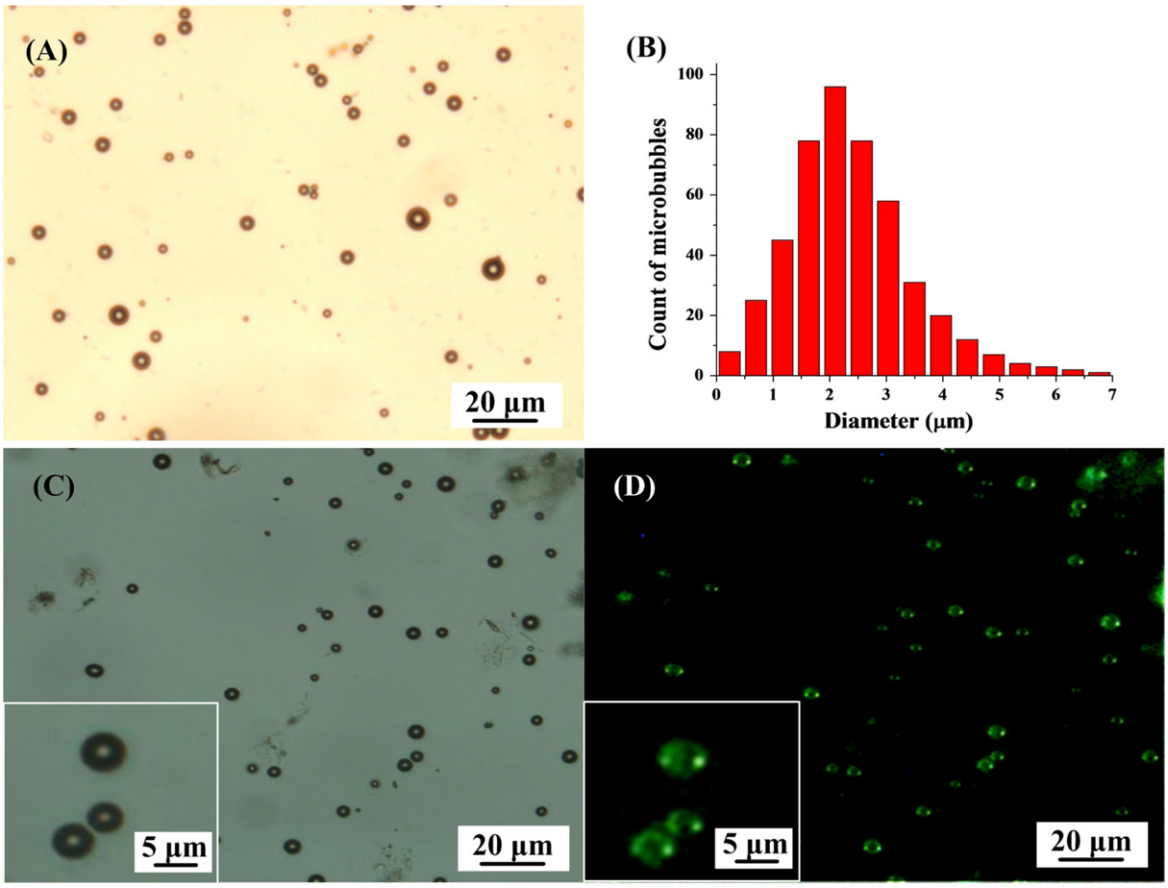

Figure 3. The morphology of MBs. (a) Imaging of ST68 MBs. (b) Size distribution of ST68 MBs; UCNP@ST68 MBs observed under an optical microscope, (c) without and (d) with excitation wavelength of the 980 nm laser diode.

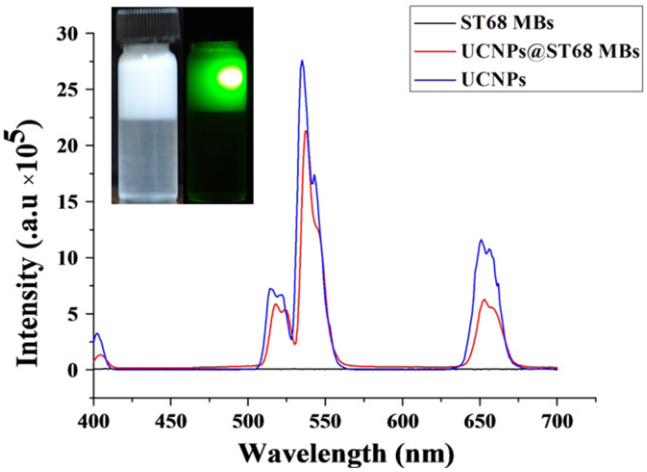

Figure 4. Fluorescence spectrum of ST68, UCNPs, and UCNP@ST68. Inset shows UCNP@ST68 MBs (left) and fluorescence image of UCNP@ST68 MBs (right).

(figure 4 inset). Besides, in our experimental process, we completed fluorescence microscope imaging and ultrasound imaging first. The inset of figure 4 was taken on the third day after preparation, which indicates that the combination between the MB and UCNP is stable. To observe the fluorescence intensity of samples, we collect the fluorescence spectrum of ST68 MBs, PAA-UCNPs, and UCNP@ST68 MBs (figure 4). No fluorescence emission can be observed for ST68 MBs subjected to NIR excitation. According to the literature, ST68 MBs possesses a emission peak at 400 nm when excited by ultraviolet light [17]. We therefore demonstrate that NIR excitation avoids fluorescence from MBs. While two emission peaks could be observed centered at 540 and 650 nm from PAA-UCNPs, the position of which is consistent with emission from $NaYF_4$:Er/Yb nanoparticles. It could be observed that the spectrum of UCNP@ST68 MBs perfectly matched the PAA-UCNPs, demonstrating the successful adsorption of UCNPs on the surface of MBs. To verify the efficiency of UCNPs coating to MBs, we compared the fluorescence intensity between PAA-UCNPs and UCNP@ST68 MBs. The concentration of PAA-UCNPs used in this experiment is equal to the concentration of PAA-UCNPs before assembly. The fluorescence intensity before and after assembly appears to be at the same level, which reveals negligible loss of PAA-UCNPs in the assembly process (figure 4).

As ultrasound contrast agents, MBs should exhibit an excellent echo property in the presence of diagnostic ultrasound for clinical application. Thus, it is necessary to maintain the echogenicity of MBs to the maximum extent after the modification with UCNPs. To test the echogenicity of MBs, we employed a latex tube in the water tank to simulate the blood vessels [37, 38]. We injected different samples into the

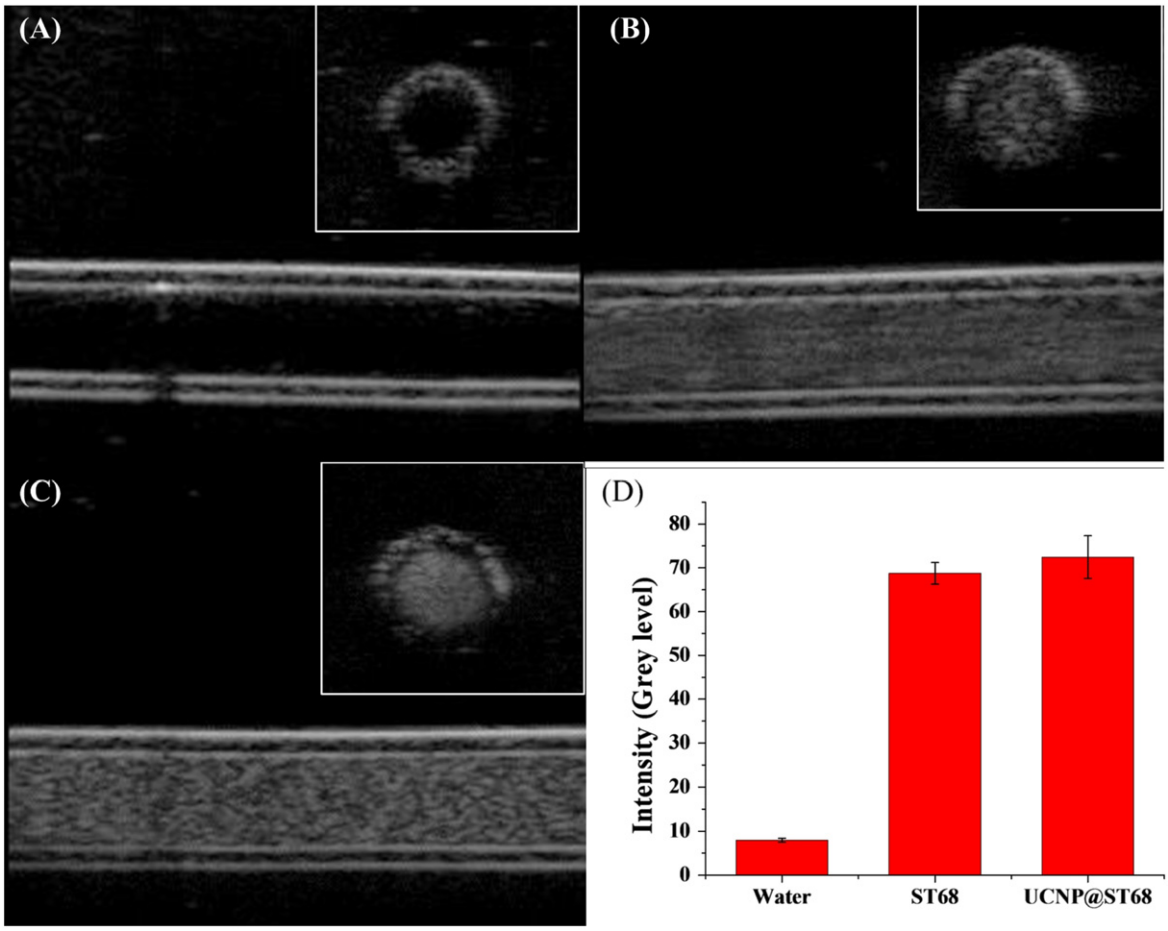

Figure 5. Ultrasound image of latex tube by injecting different agents. (a) Imaging of tube filled with water. (b) Imaging of tube filled with ST68 MBs. (c) Imaging of tube filled with UCNP@ST68 MBs. (d) Quantitative analysis of the intensity of different samples (the concentration of MBs in (b) and (c) are fixed as 10^6 bubbles/mL).

tube and collected its B-mode ultrasound images, as shown in figure 5. There is obviously no contrast enhancement in the B-mode ultrasound images when water is injected into the tube (figure 5(a)). Then ST68 MBs and UCNP@ST68 were diluted to about 10^6 bubbles/mL and were injected into the tube separately (the concentration is calculated by hemocytometer). Immediately, the inner space of the tube showed strong ultrasound echo enhancement when ST68 MBs (figure 5(b)) and UCNP@ST68 MBs (figure 5(c)) were injected. Besides providing both upconversion fluorescence signal and ultrasound contrast enhancement, we observed a slightly enhanced ultrasound signal for UCNP@ST68 MBs as compared with ST68 MBs under the same conditions (figures 5(b) and (c)). This enhanced ultrasound signal maybe be attributed to presence of UCNPs on the surface of the MBs that cause bubble asymmetry, and the subsequent change in the oscillation frequency results in an increased scattering cross-section [39]. Quantitative analysis of the ultrasound signal intensities from water, ST68 MBs, and UCNP@ST68 MBs are shown in figure 5(d). The intensity of UCNP@ST68 MBs is higher than that of ST68 MBs with both concentrations fixed as 10^6 bubbles/mL.

The appropriate ultrasound contrast agent should possess the following characteristics: (i) nontoxic and biocompatible, (ii) suitable size to pass through the pulmonary, cardiac, and capillary circulations, (iii) stable for storing and recirculation. ST68 MBs were generated from materials including Span 60, Tween 80, and SF_6. These materials have been proved to be nontoxic and biocompatible [17]. In addition, the average size of MBs is about 2 μm, which is suitable to pass through the pulmonary circulation. Experimental results show that ST68 MBs are able to remain stable in PBS for about 4 weeks without significant decrease in concentration, while the UCNP-modified ST68 MBs was found to be stable for about 2 weeks.

MBs are known to alternately contract and expand when in an acoustic field, a phenomenon called cavitation. At low acoustic intensity, MBs grow and shrink rhythmically and symmetrically around their equilibrium size. At high acoustic intensity, however, the expansion and contraction of the MBs usually become unequal and markedly increased, leading to their destruction [40]. By using this phenomenon, THE ultrasound-targeted MB destruction (UTMD) technique was used for targeted drug/gene targeted delivery. The UCNP-modified MBs have great potential to deliver UCNPs using the UTMD technique for targeted fluorescence imaging. For potential clinical applications, the UCNP-modified MBs could be intravenously injected into patients and targeted to

the lesion (such as a tumor or atherosclerotic plaque) and the MBs could be destroyed by a high intensity ultrasound wave, then UCNPs would be locally unloaded and concentrated around the lesion site, which could mark and track lesions. In a word, UCNP-modified MBs would act as a promising controlled release system for ultrasound triggered targeted delivery of UCNP for fluorescent imaging. Compared with the target-ready contrast agent [41], UCNP@ST68 MBs are a kind of bimodal imaging contrast agent without a targeting function due to the lack of targeting moieties. Combing a bimodal imaging contrast agent with a targeting function should have a broad prospect for targeting purposes.

4. Conclusion

The UCNPs-modified MBs were successfully fabricated by stepwise LbL assembly of PAH- and PAA-modified UCNPs onto the surface of MBs. The obtained bimodal contrast agent renders both ultrasound and fluorescence imaging modalities. The bimodal contrast agent exhibits suitable size, a low polydispersity, and stability. For ultrasound mode, the bimodal contrast agent shows a slightly enhanced ultrasound signal, due to the change of bubble asymmetry as a result of UCNPs coating. For fluorescence mode, the bimodal contrast agent presents high fluorescence intensity from UCNPs. The novel fluorescence/ultrasound contrast agent shows promising application in bimodal imaging. Besides, the proposed method is simple and universal, enabling easy assembly of other charged materials (e.g., drugs or genes) onto the surface of MBs to obtain a multi-function contrast agent.

Acknowledgments

This work was financially supported by the International Science and Technology Cooperation Program of China (2013DFG02930), National Key Scientific Apparatus Development of Special Item (2013YQ190467), and the Fundamental Research Funds for the Central Universities (2012jdhz46). M L is supported by a scholarship from the China Scholarship of Council. The TEM work was done at the International Center for Dielectric Research (ICDR), Xi'an Jiaotong University, Xi'an, China. The authors also thank Dai Yan Zhu, Lu Lu, and Ma Chuan Sheng for their help using TEM.

References

[1] Janib S M, Moses A S and MacKay J A 2010 Imaging and drug delivery using theranostic nanoparticles *Adv. Drug Delivery Rev.* **62** 1052–63
[2] Wen Q *et al* 2014 Ultrasound contrast agents and ultrasound molecular imaging *J. Nanosci. Nanotechnol.* **14** 190–209
[3] Anderson C R *et al* 2011 Ultrasound molecular imaging of tumor angiogenesis with an integrin targeted microbubble contrast agent *Investigative Radiol.* **46** 215
[4] Faez T, Emmer M, Kooiman K, Versluis M, van der Steen A and de Jong N 2013 20 years of ultrasound contrast agent modeling *IEEE Trans. Ultrason. Ferroelect. Frequency Control* **60** 7–20
[5] Cosgrove D 2006 Ultrasound contrast agents: an overview *Euro. J. Radiol.* **60** 324–30
[6] Stride E and Edirisinghe M 2008 Novel microbubble preparation technologies *Soft Matter* **4** 2350–9
[7] Klibanov A 2009 Preparation of targeted microbubbles: ultrasound contrast agents for molecular imaging *Med. Biol. Eng. Comput.* **47** 875–82
[8] Stride E and Edirisinghe M 2009 Novel preparation techniques for controlling microbubble uniformity: a comparison *Med. Biol. Eng. Comput.* **47** 883–92
[9] Stewart V R and Sidhu P S 2006 New directions in ultrasound: Microbubble contrast *Br. J. Radiol.* **79** 188–94
[10] Lentacker I, De Smedt S C and Sanders N N 2009 Drug loaded microbubble design for ultrasound triggered delivery *Soft Matter* **5** 2161–70
[11] Lindner J R 2004 Microbubbles in medical imaging: current applications and future directions *Nat. Rev. Drug Discov.* **3** 527–33
[12] Cui W *et al* 2013 Neural progenitor cells labeling with microbubble contrast agent for ultrasound imaging *in vivo Biomater.* **34** 4926–35
[13] Weller G E R *et al* 2003 Ultrasound imaging of acute cardiac transplant rejection with microbubbles targeted to intercellular adhesion molecule-1 *Circulation* **108** 218–24
[14] Yang F *et al* 2009 Superparamagnetic iron oxide nanoparticle-embedded encapsulated microbubbles as dual contrast agents of magnetic resonance and ultrasound imaging *Biomater.* **30** 3882–90
[15] Yang F *et al* 2011 Controlled release of Fe3O4 nanoparticles in encapsulated microbubbles to tumor cells via sonoporation and associated cellular bioeffects *Small* **7** 902–10
[16] Lin C A J *et al* 2012 Rapid transformation of protein-caged nanomaterials into microbubbles as bimodal imaging agents *ACS Nano* **6** 5111–21
[17] Hengte K *et al* 2009 Quantum-dot-modified microbubbles with bi-mode imaging capabilities *Nanotechnology* **20** 425105
[18] Yang F *et al* 2013 Silver nanoparticle-embedded microbubble as a dual-mode ultrasound and optical imaging probe *ACS Appl. Mater. Interfaces* **5** 9217–23
[19] Klibanov A L 2009 Preparation of targeted microbubbles: ultrasound contrast agents for molecular imaging *Med. Biol. Eng. Comput.* **47** 875–82
[20] Yang Y 2014 Upconversion nanophosphors for use in bioimaging, therapy, drug delivery and bioassays *Microchimica Acta* **181** 263–94
[21] Liu L, Miao Q and Liang G 2013 Quantum dots as multifunctional materials for tumor imaging and therapy *Mater.* **6** 483–99
[22] Chibli H *et al* 2011 Cytotoxicity of InP/ZnS quantum dots related to reactive oxygen species generation *Nanoscale* **3** 2552–9
[23] Lin M *et al* 2012 Recent advances in synthesis and surface modification of lanthanide-doped upconversion nanoparticles for biomedical applications *Biotechnol. Adv.* **30** 1551–61
[24] Ong L C *et al* 2014 Bacterial imaging with photostable upconversion fluorescent nanoparticles *Biomater.* **35** 2987–98
[25] Han J *et al* 2014 Upconversion nanoparticles for ratiometric fluorescence detection of nitrite *Analyst* **139** 3032–8
[26] Ang L Y *et al* 2011 Applications of upconversion nanoparticles in imaging, detection and therapy *Nanomedicine* **6** 1273–88
[27] Feng A L *et al* 2015 Distance-dependent plasmon-enhanced fluorescence of upconversion nanoparticles using polyelectrolyte multilayers as tunable spacers *Sci. Rep.* **5** 7779

[28] You M *et al* 2015 Inkjet printing of upconversion nanoparticles for anti-counterfeit applications *Nanoscale* **7** 4423–31
[29] Basude R, Duckworth J W and Wheatley M A 2000 Influence of environmental conditions on a new surfactant-based contrast agent: ST68 *Ultrasound Med. Bio.* **26** 621–8
[30] Zhou M, Cavalieri F and Ashokkumar M 2011 Modification of the size distribution of lysozyme microbubbles using a post-sonication technique *Instrum. Sci. Tech.* **40** 51–60
[31] Zha Z, ZhangS W S, Qu E, Ke H, Wang J and Dai Z 2013 Targeted delivery of CuS nanoparticles through ultrasound image-guided microbubble destruction for efficient photothermal therapy *Nanoscale* **5** 3216–9
[32] Inaba Y and Lindner J R 2012 Molecular imaging of disease with targeted contrast ultrasound imaging *Transl. Res.* **159** 140–8
[33] Fan X *et al* 2013 Experimental investigation of the penetration of ultrasound nanobubbles in a gastric cancer xenograft *Nanotechnology* **24** 325102
[34] Xu R X 2011 Multifunctional microbubbles and nanobubbles for photoacoustic imaging *Contrast Media Mol. Imaging* **6** 401–11
[35] Xing Z *et al* 2010 Novel ultrasound contrast agent based on microbubbles generated from surfactant mixtures of Span 60 and polyoxyethylene 40 stearate *Acta Biomater.* **6** 3542–9
[36] Sheeran P S *et al* 2011 Decafluorobutane as a phase-change contrast agent for low-energy extravascular ultrasonic imaging *Ultrasound Med. Biol.* **37** 1518–30
[37] Liu T Y *et al* 2013 A novel ultrasound-triggered drug vehicle with multimodal imaging functionality *Acta Biomater.* **9** 5453–63
[38] Williams R, Gorelikov I and Chaudhuri J 2009 Nanoparticle-loaded perflulorocarbon droplets for imaging and therapy, *Ultrasonics Symp. IUS), 2009 IEEE Int.* pp 5–8
[39] Park J I *et al* 2010 Microbubbles loaded with nanoparticles: a route to multiple imaging modalities *ACS Nano* **4** 6579–86
[40] Ay T *et al* 2001 Destruction of contrast microbubbles by ultrasound: effects on myocardial function, coronary perfusion pressure, and microvascular integrity *Circulation* **104** 461–6
[41] Helfield B L and Goertz D E 2013 Nonlinear resonance behavior and linear shell estimates for Definity and MicroMarker assessed with acoustic microbubble spectroscopy *J. Acoust. Soc. Am.* **133** 1158–68